High-resolution inelastic neutron scattering from water in mesoporous silica

F. Mansour,[1] R. M. Dimeo,[2] and H. Peemoeller[1,*]
[1]*Department of Physics, University of Waterloo, Waterloo, Ontario, Canada N2L 3G1*
[2]*NIST Center for Neutron Research, National Institute of Standards and Technology, 100 Bureau Drive, Stop 8562, Gaithersburg, Maryland 20899-8562*

(Received 30 April 2001; revised manuscript received 22 May 2002; published 22 October 2002)

High-resolution inelastic neutron scattering measurements of the molecular dynamics of water confined to a porous host, the molecular sieve known as MCM-41, which has a hexagonal array of parallel pores with average pore diameter of 27 Å, are reported. Previous neutron measurements probing higher-energy transfers, and thus shorter time scales, have been analyzed with both a rotation-translation diffusion model and a stretched exponential intermediate scattering function. The dynamics on longer time scales presented here are modeled well with a stretched exponential relaxation in a confining geometry. The observed molecular dynamics of water are three orders of magnitude slower than has been previously reported for water confined in MCM-41.

DOI: 10.1103/PhysRevE.66.041307 PACS number(s): 81.05.Rm, 68.08.−p

I. INTRODUCTION

The effects of confinement on the molecular properties of water have attracted a lot of interest in the past few decades [1–11]. Understanding the behavior of this fascinating hydrogen bonded fluid upon confinement is of value to a vast array of problems ranging from oil recovery and geochemical applications to biophysical interactions, medical imaging, colloid and interface chemistry, and food product quality.

It is accepted that water molecules access a large range of possible motional frequencies depending on the nature of the confining medium. Results from quasielastic neutron scattering show the characteristic relaxation time for water molecules in pores as small as 20 Å in diameter to be of the order of a few picoseconds [4], only a few times slower than the correlation time for bulk water [12]. On the other extreme, nuclear magnetic relaxation results reveal correlation times on the order of a few microseconds in pores as large as a few hundred angstroms [3]. Using neutron spin echo, Swenson *et al.* recently measured relaxation times in the 10^{-10}–10^{-6} s range for water confined in vermiculite clay [13].

The early 1990s witnessed the discovery of family of mesoporous molecular sieves known as M41S [14] which has since been the center of some attention in the literature due to its possible uses in a wide variety of processes [14,15]. One member of the family, MCM-41, consists of a hexagonal crystalline arrangement of paraxial channels. The material can be produced with finely tuned pore diameters within the 16–100 Å range as well as a very high surface area (in excess of 1000 m^2/g). The material has spawned a revolution in catalysis. The extremely high surface area allows for superb catalytic conductivity, and the relatively large pore size compared to conventional zeolites (typically less than 10 Å) allows the incorporation of large active complexes in the pores. Thin films of the material can be produced with pore channels either parallel or perpendicular to the substrate used, thus allowing for order on larger scales, a highly desirable property. Many potential applications of the material involve an aqueous phase. In such cases water-surface interactions play an important role in determining the properties of the systems of interest and in controlling catalysis, chemical reactions, and water mediated biological interactions. In addition, in such restricted geometry, the molecular and bulk properties of water (e.g., structure and dynamics, phase transitions, freezing behavior) are modified due to a combination of water-surface interaction, global confinement effects and sample morphology [16–19].

Previous neutron scattering measurements of confined water were carried out using time-of-flight spectrometers with energy resolution of order 10–100 μeV yielding information about dynamics in the range of 1–100 ps [1,2,4,5]. These previous studies on water in confinement have concluded that motion of water can be described as single-particle diffusion with a correlation length of a few angstroms. This value of a confining radius was arrived at by various research groups regardless of the pore size or geometry used [4,5,20,24]. This result comes about due to instrument limitations in sampling time scales that allow water molecules to diffuse only within such small radii.

Most porous materials have imperfect pore structures. Materials like Vycor and controlled porous glasses (CPG) are known to have interconnected pores with low monodispersity, and a poorly defined pore geometry. In these more random confining geometries it is difficult to disentangle the relevant features of the host material that yield the differences in the molecular dynamics of the bulk and confined systems. It is of both fundamental and practical interest to determine the effects of the interconnectedness of the pore network, the pore size distribution, the presence of strong surface interactions, and the absolute pore size on the dynamics of water.

In this paper we present results of a series of inelastic incoherent neutron scattering measurements of water in MCM-41. Previous measurements on water in MCM-41 suggested dynamics on time scales of picoseconds. Here we extend these measurements using very high-resolution neutron spectroscopy and find that the confined water exhibits

*Author to whom correspondence should be addressed.

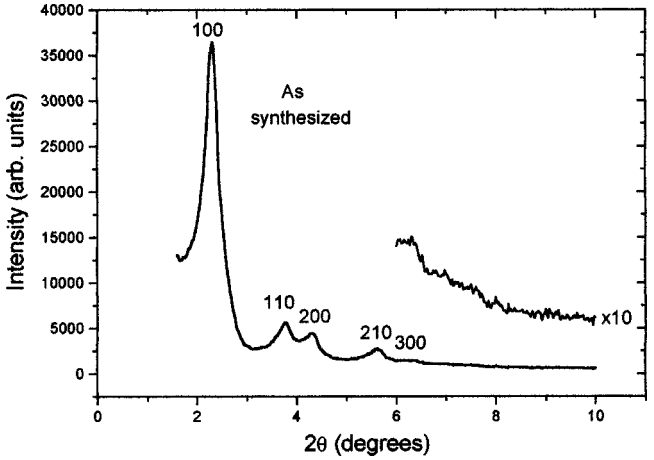

FIG. 1. X-ray diffraction pattern of MCM-41 as synthesized for this study. The narrow width of the 110 peak is evidence of well developed powder particles. The higher-order peaks reflect the high crystallinity of the porous particles.

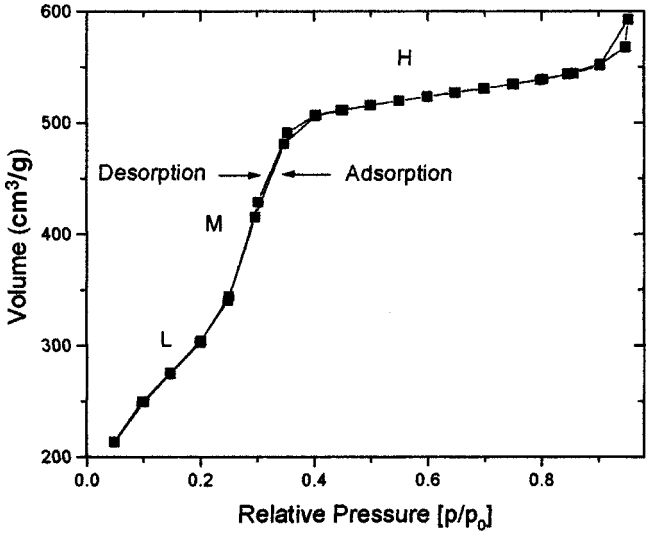

FIG. 2. Nitrogen adsorption-desorption isotherm for calcined MCM-41. The isotherm shows no evidence of hysteresis. The sharp middle region demonstrates the narrow pore size distribution of the material.

dynamics three orders of magnitude slower than found in the previous measurements. This paper is organized as follows. Section II describes the synthesis and characterization of the porous host MCM-41. In Sec. III we discuss the neutron scattering measurement details. In Sec. IV the data analysis and results are presented, including a detailed description of the theoretical model used in fitting the data. Finally, we summarize our findings in the concluding Sec. V.

II. SYNTHESIS AND CHARACTERIZATION OF MCM-41

Fumed silica powder (99.8%, metal free, particle size 0.07 μm) and tetramethyl ammonium hydroxide pentahydrate (TMAOH, 97%) were obtained from Sigma. Cetyltrimethyl ammonium bromide (CTABR, 99%) was obtained from Aldrich. TMAOH and CTABR were dissolved in distilled deionized water in a 250 ml beaker while stirring with a magnetic stirrer (500 rpm) at 30 °C until a clear solution was obtained. The silica powder was then added and the mixture stirred for 3 h at 30 °C. The final molar composition of the material was 1.0 SiO_2, 0.19 TMAOH, 0.27 CTABR, 40 H_2O [10] and it contained 200 g of water. The mixture was aged for 24 h at room temperature and transferred into a stainless steel Viton-lined autoclave. The mixture was allowed to react in a furnace at 125 °C for 68 h, after which the autoclave was cooled under running water. The solid material was recovered by filtration, washed extensively in distilled deionized water, and dried at 45 °C overnight. Finally, calcining the sample at 650 °C for 8 h removed the organic template material.

X-ray diffraction (XRD) measurements were carried out with the Cu $K\alpha$ radiation from a Siemens D5000 [38] diffractometer operating at 40 kV and 30 mA using 0.025° steps and a 2 s step time. Nitrogen adsorption and desorption measurements were carried out on a Quantochrome [38] Autosorb automated gas sorption system at 77 K with an outgas temperature of 473 K.

Figure 1 shows the XRD powder pattern as a function of 2θ. The peaks in the diffraction pattern are labeled according to a hexagonal unit cell. The crystallinity of the sample comes from a hexagonal distribution of one-dimensional channels rather than from a crystalline arrangement of atoms within the sample. The rarely observed 300 peak can be seen in the magnified portion of the pattern (inset Fig. 1). The wall-to-wall distance in the as-synthesized sample is 38.9 Å, which contracts to 35.43 Å after calcining.

The N_2 adsorption isotherms are shown in Fig. 2. The overlay of the adsorption-desorption phase isotherms indicates no significant hysteresis. The linear increase over the low-pressure region (L) of the isotherm ($P/P_0 < 2.5$) is accounted for by the adsorption of a thin layer of gas on the pore walls. The isotherm shows an inflection characteristic of capillary condensation in the intermediate-pressure region (M). The sharp increase in the volume of adsorbed N_2 in that region is indicative of the narrow distribution of the pore diameters. The increase in adsorbed volume in the high-pressure region (H) is attributed to multilayer condensation at the outer surface. The pore size distribution is calculated using the Kelvin equation [21]. The narrow pore size distribution is centered at a diameter of 27.5 Å and the total surface area was calculated to be 850 m^2/g.

III. NEUTRON SCATTERING MEASUREMENT DETAILS

Neutron scattering measurements were carried out at the NIST Center for Neutron Research on the high-flux backscattering spectrometer (HFBS) [22]. The HFBS is a high-energy-resolution backscattering spectrometer in which the incident neutron energy is varied via Doppler shifting the neutrons about a nominal incident wavelength of 6.271 Å. After scattering from the sample only neutrons with a fixed final energy are received in the detectors as determined by Bragg reflection from a large crystal analyzer system. The instrument operated with a dynamic range of ± 10 μeV. The energy resolution of the instrument was obtained by scatter-

ing from the sample plus sample holder at a temperature of 113 K. The data were collected for five temperatures between 213 and 300 K, and 16 wave vector transfer (or Q) values ranging from 0.25 to 1.75 $Å^{-1}$. The resolution of the instrument, 0.80 μeV full width at half maximum, was obtained by fitting a single Gaussian function to the elastic scattering at 113 K. The HFBS therefore can probe dynamics in the nanosecond range, a thousand times slower than the dynamics in bulk water. Previous neutron scattering measurements of water in confinement have concluded that the dynamics of water slow down by less than one order of magnitude from the dynamics in the bulk [4,5]. The water-saturated MCM-41 was placed in a slab-geometry thin-walled aluminum sample holder, sealed with an indium O ring, and mounted onto a closed-cycle refrigerator. The temperature was controlled to within ± 0.05 K.

IV. DATA ANALYSIS AND RESULTS

In an inelastic neutron scattering experiment, one measures the partial differential scattering cross section (PDSCS) $d^2\sigma/d\Omega\, dE$, where E is the energy transfer to the sample and $d\Omega$ is the solid angle into which the neutron is scattered [23]. The PDSCS, which depends on experimental and sample details, is related to the sample scattering function $S(Q,E)$, which depends on the sample only. This relationship is given by

$$\frac{d^2\sigma}{d\Omega\, dE} = N \frac{\sigma}{4\pi} \frac{\kappa}{\kappa_i} S(Q,E), \tag{1}$$

where N is the number of scattering centers in the collision, κ is the scattered wave vector, κ_i is the incident wave vector, and σ is the scattering cross section of the scatterer. The sample scattering function is related to the intermediate scattering function (ISF) $I_s(Q,t)$ via Fourier transformation in time, which can often be calculated with a theoretical model.

Inelastic neutron scattering data from water are typically analyzed using models that take into account contributions from the vibrational modes in water combined with rotational and translational diffusion contributions. The resulting structure factor is a convolution of the three structure factors corresponding to each type of motion. The motion of water molecules in the bulk at room temperature can be described as a normal stationary Markovian random process. The position and orientation of an individual water molecule depends only on the time and distance separating it from its previous position. The motion does not carry information about initial conditions. The correlation function of water molecular motion in this case falls off exponentially with time. The exponential model has been typically adopted for analyzing relaxation data for water in confinement.

The mode coupling theory of liquids has been widely used recently in developing models to study the behavior of glass-forming liquids [25] and supercooled water [26]. It relies on the transient cage effect defined as the trapping of water or liquid molecules in cages upon supercooling of the fluid. One of its predictions is the existence of a critical temperature T_c identified as the singularity temperature for water, $T_s \sim 228$ K. Upon approaching that temperature from above, the cage relaxation time becomes longer and longer until it reaches infinity at T_s, at which point the liquid reaches a state of structural arrest. This prediction is in striking agreement with the predictions from molecular dynamics (MD) simulations of the simple point charge-extended (SPC/E) water model [26]. The MD simulations also predict a critical or singularity temperature at which water undergoes a structural arrest and where the diffusion constant becomes zero. This occurs at $\sim 49°$ below the temperature of maximum density for the SPC/E model. It also signifies the onset of vitrification as a result of a kinetic glass transition [9]. The main evidence supporting the existence of the singularity temperature comes from the power law dependence of several water relaxation parameters on temperature [27]. Since the singularity temperature is experimentally inaccessible in bulk water, it becomes necessary to look at water under confinement conditions that will allow sufficient supercooling. Chen *et al.* provide a detailed derivation for the single-particle ISE as a result of applying the mode coupling theory (MCT) to supercooled water [26].

Zanotti *et al.* have recently applied the predictions of MCT to supercooled water confined in porous glass. An appropriate ISF would then be obtained by multiplying the appropriate expression for a particle confined to a cage [5] by a stretched exponential factor to capture both the long and short time evolution of the relaxation.

After making some relevant approximations the final ISF has the following form [5,26]:

$$I_s(Q,t) = A(Q) \exp\left[-\left(\frac{t}{\tau} \right)^{\beta} \right]. \tag{2}$$

In Eq. (2) $A(Q)$ is the elastic ISF (EISF) obtained for water molecules confined either to a sphere or to a hydrogen bonded cage, depending on the model used. In this paper, however, we do not rely on any preexisting model to obtain the EISF; a very different explanation of the origin of the EISF used in our model is given below.

An alternative approach to the study of supercooled water comes from the percolation or transient gel model [28–31] and the lattice fluid [32] model, which do not include a singularity temperature. A necessary outcome of the percolation model is a continuous distribution of correlation or relaxation times in supercooled water. A continuous distribution of relaxation times is observed in glasses and glass-forming liquids. Confinement of water results in a molecular structure and dynamics similar to those observed in supercooled bulk water [26]. Hence, under proper confinement and reduced temperature conditions one should be able to access the region below the kinetic glass transition temperature. As a matter of fact, water molecules on the surface of proteins are known to exhibit glasslike behavior [33].

Further evidence comes from experiments done on the freezing of confined water which is widely believed to start from the middle of the confining region where free water exists and then proceed outward toward the wall. The so-called surface water, a monolayer or so of water molecules closest to the surface, is believed to be nonfreezable [16,34]. Freezing measurements can be used to measure the pore size

distribution of porous materials [34]. These often reveal a sharp transition near the characteristic freezing temperature of the water in the pores. The sharpness of the transition is a good indicator of the monodispersity of the pore size distribution.

As the temperature is lowered further below the characteristic freezing temperature, a smooth and slow continuous transition is observed. This is associated with surface water molecules in the sample. The pore size calculations must take into account the thickness of the nonfreezable water layer [34]. The technique works extremely well but only down to certain pore sizes [16]. The reason can be attributed to the absence of free water in very small pores and the fact that all the water behaves more or less like surface, nonfreezable water. Morishige and Kawano used x-ray diffraction measurements to characterize the freezing and melting and phase behavior of water confined to the pores of different pore size MCM-41. Most of the samples showed the anticipated sharp transition near the expected freezing temperature. Their smallest pore size sample, $R=12$Å, similar to the pore size of the sample we have used in this study, does not show any sign of a sharp transition near the anticipated freezing point ($\sim$223 K from the Kelvin equation). Rather, there is continuous transition over the 200–260 K range. This indicates that the water in the pores exists well within the glassy phase. This is expected because of the low temperatures (223–260 K) at which the results were obtained, in conjunction with the very small size of the confining pores, which would effectively result in a further, more severe supercooling of the water in the sample. Under these conditions, the water dynamics can be characterized by a distribution of correlation times $g\ (\ln\tau)$ [35], as for other glasses. The relaxation process is well represented by the Kohlrauch-Williams-Watts (KWW) model, and an appropriate single-particle ISF can be written as

$$I_s(Q,t)=A^*(Q)\exp\left[-\left(\frac{t}{\tau}\right)^{\beta}\right] \tag{3}$$

where β is the stretch factor.

It is worth noting that, although this ISF has exactly the same form as the ISF in Eq. (2), which was obtained by using MCT predictions after appropriate approximations were made, the underlying principles are different, as is the significance of the elastic structure factor. One would not expect the mode coupling theory to be an appropriate model for the water in such small pores, because the appropriate regime for MCT is restricted to weakly supercooled states [36]. In addition, excluding the surface water, one cannot expect to have more than four or five layers of water molecules between the walls, so that well ordered cages of water (e.g., pentamers) are unlikely to form.

There are two factors contributing to the modified elastic structure factor $A^*(Q)$ in Eq. (3). NMR evidence reveals water molecule dynamics in the same sample [37] and in similar samples [3] in the microsecond range, which would give an elastic contribution to the structure factor. Another contribution comes from the protons of the surface hydroxyl groups of the pore walls, which are also expected to have very slow dynamics relative to the observed time scale.

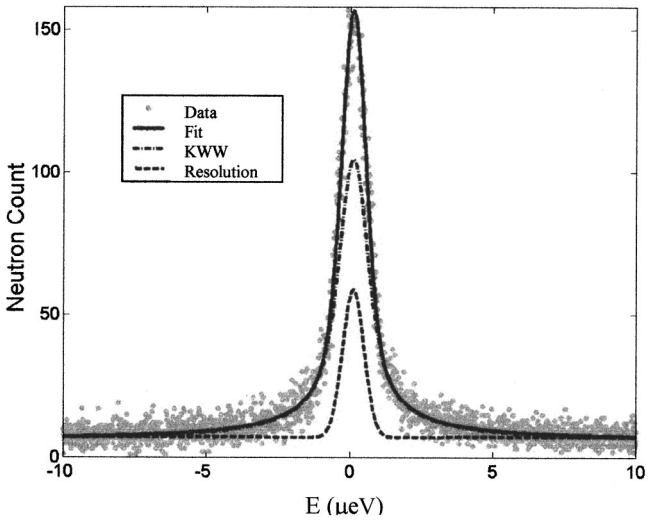

FIG. 3. High-resolution inelastic neutron scattering data taken at 223 K at a Q of 1.1 Å^{-1}. The open circles are the neutron counts, and the solid line is the best fit to the data. The solid line is a convolution of the resolution function with a stretched exponential function, which are also shown individually. The convolution was carried out according to Eq. (5).

The inelastic spectra were fitted to a scattering function consisting of the sum of a δ function and the Fourier transform $\mathcal{F}$ of a stretched exponential decay convoluted with the resolution function of the instrument,

$$S(Q,E)=[\,\delta(E)+A^*(Q)\mathcal{F}(S_e)\,]\otimes R(Q,E), \tag{4}$$

which is the Fourier transform of the following function in the time domain:

$$\Phi(Q,t)=\left\{R(Q)\exp\left[-\left(\frac{t}{\tau_0}\right)^2\right]+A^*(Q)\exp\left[-\left(\frac{t}{\tau_0}\right)^2\right]\exp\left[-\left(\frac{t}{\tau}\right)^{\beta}\right]\right\}\times\exp[\,i\varphi(Q)t\,]. \tag{5}$$

The first term in the square brackets is an amplitude multiplying the Fourier transform of the resolution function of the instrument, best represented by a single Gaussian decay. The value of τ_0 was determined at each Q value from the 113 K data. The second term in the brackets is the ISF for water. The last term in the equation is a complex phase factor to take care of the zero-frequency offset in the spectrum. The Fourier transform was carried out numerically such that each data point in the frequency domain was assigned a corresponding point in the time domain.

A sample spectrum is shown in Fig. 3. The points represent the data at $Q=1.1$ Å^{-1} and the solid line is the fit using the model given in Eq. (5). The overall relaxation time and the stretch factor β obtained from the fit are presented in Table I. The dependence of the relaxation rate $(1/\tau)$ on Q for

TABLE I. Relaxation times and stretch factors as a function of Q and T. The top of the table also contains the values of the power of the power law dependence of the relaxation rate at each temperature. The empty spaces correspond to the points where the signal to noise ratio was poor or where the sample orientation resulted in significant neutron absorption. The correlation times are in nanoseconds. Values of β that are greater than 1 have been discarded.

	T (K)							
	223 $\gamma=1.2\pm0.1$		227 $\gamma=1.58\pm0.14$		230 $\gamma=1.72\pm0.36$		260 $\gamma=2.37\pm0.91$	
Q (Å^{-1})	τ	β	τ	β	τ	β	τ	β
0.25	8.61		7.83	0.71	5.48	0.10	4.9	0.37
0.365	6.68	0.69	6.64	0.55	1.79	0.58	1.78	0.30
0.469	3.91		4.27	0.93	2.78	0.81	0.80	0.72
0.745	2.69	0.42	1.62	0.66	0.96	1.05	0.29	0.23
0.991	1.90	0.66	1.05	0.67	0.39	0.82	0.02	0.33
1.106	1.38	0.46	0.94	0.75	0.13	0.61		
1.217	0.44	0.57	1.48	0.84	0.18	0.49		
1.32	0.35	0.38	0.41	0.58			0.38	0.33
1.42			0.16	0.38	0.28	0.55		
1.598	0.03	0.33						

the various temperatures is presented in Fig. 4. The relaxation rate increases with increasing Q, and the best fit to the data reveals a power law dependence of the relaxation rate on Q, in keeping with previous results obtained for water confined in Vycor [5]. There is some deviation from the DQ^2 scattering law as the power takes on values between 1.2 and 2.4 (Table I), increasing as the temperature increases.

Previously reported values for the power γ are typically larger than 2 [5,35]; for our data this is also true for the highest temperature. The data taken at 223, 227, and 230 K give values for γ that are less than 2. This is an interesting result, and further investigation is warranted to find the physical reasoning behind such behavior. It should be noted that most measurements on supercooled water rarely venture near the critical temperature of ~228 K, and the three anomalous temperatures in this case are either very close to or below that value.

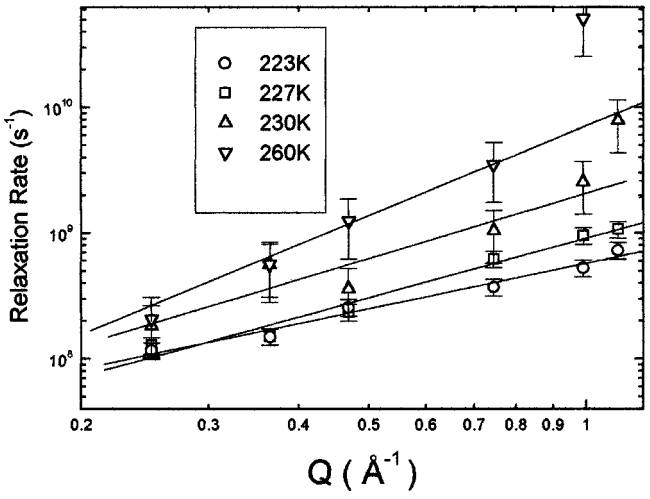

FIG. 4. The relaxation rate $(1/\tau)$ for water as a function of Q. The log-log plot shows evidence of a power law dependence. The Q range shown is 0.25–1.2 Å^{-1}.

One might also be inclined to conclude that such a behavior could be attributed to the fact that the theoretical freezing temperature of the pores is being approached, as predicted by the Kelvin equation. Although water molecules are in the glassy phase, a significant portion is expected to be frozen [16,34]; this is a very interesting region where water is most likely making the smooth transition from the liquid to the frozen state. In order to delineate the two effects it would be desirable to observe water near the freezing temperature in a larger pore size and near the critical temperature in a smaller pore size.

The data also show a sharp increase in slope in the log-log plot of the relaxation rate vs Q at around $Q=1.2$ Å^{-1}. No quantitative conclusions can be made due to the very poor signal to noise ratio in that Q range. It does, however, seem to indicate a further divergence at higher Q values from the hydrodynamic behavior of water, which one should be able to recover at sufficiently low Q values in the case of the 260 K data, and, within experimental error, the 230 K data.

Figure 5 shows the stretch factor as a function of Q. Although there is a lot of uncertainty in the data, the overall trend shows that β falls significantly below 1 for large values of Q, and approaches unity for small Q values. At large values of Q the scattering probes the ideal gas behavior of the fluid. The diffusive nature of the motion is recovered for low values of Q, where the value of β approaches unity.

The fitting process depends upon the relaxation time and the stretch factor β; a more physically meaningful value of the relaxation time would have to take both variables into account. The average relaxation time can be well represented by [5]

$$\tau_a=\int_0^\infty \exp\left[-\left(\frac{t}{\tau}\right)^\beta\right]dt=\frac{\dot{\tau}}{\beta}\Gamma\left(\frac{1}{\beta}\right). \tag{6}$$

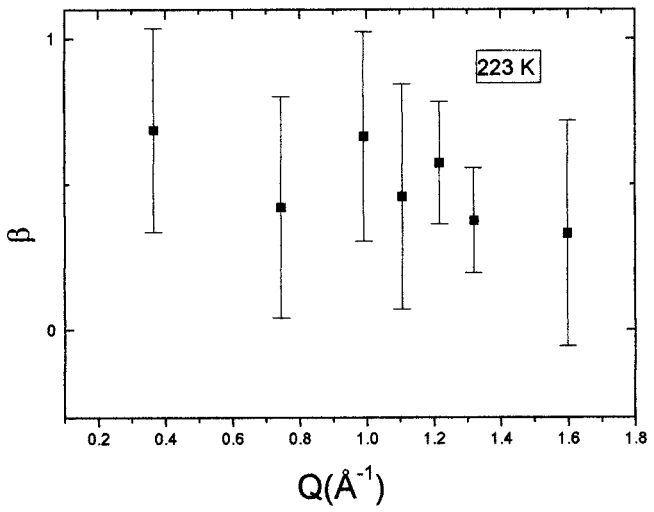

FIG. 5. Q dependence of the stretch factor β. Data were taken at 223 K. Although there is a significant uncertainty in the parameter, the trend is for β to become smaller for larger values of Q.

The dependence of the average relaxation rate $(1/\tau_a)$ on Q is shown in Figs. 6(a)–6(d). There is significant scatter in the data, due to the combined uncertainties in the value of the relaxation time, and, more importantly, the error in the stretch factor β (Fig. 5). The values of γ are all below 2 except for the data obtained at $T=260$ K, indicating again a very peculiar behavior of water at such low temperatures as discussed above.

V. CONCLUSIONS

We have used very high-resolution inelastic neutron scattering to probe the low-energy dynamics of water the motion of which is confined in a regular array of pores of MCM-41. Our results confirm earlier conclusions that models based upon Markovian processes cannot describe the molecular behavior of water in the supercooled state. The inelastic spectra are best described by Fourier transforms of stretched exponential decaying functions.

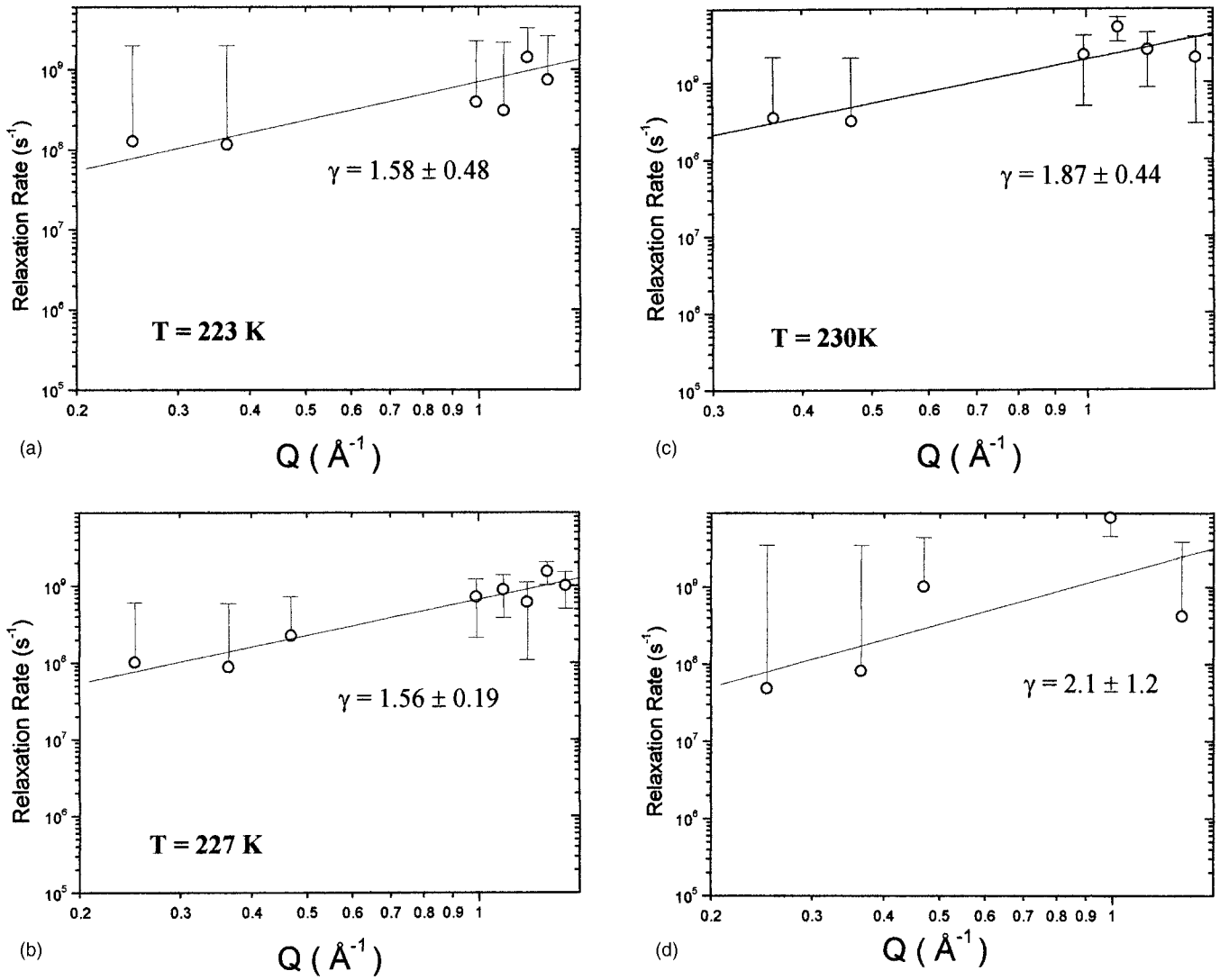

FIG. 6. The average relaxation rate $(1/\tau_a)$ for water in saturated MCM-41 as a function of Q. The average relaxation time is calculated using Eq. (6).

The mode coupling theory has been very successful in describing single-water-molecule dynamics in the weakly supercooled state. However, due to the small confining radius of the pores used in this study, a more appropriate theoretical framework would take into account the glasslike behavior of the confined water. No free water is expected to exist within such small pores. The behavior of the water molecules no longer reflects the weak supercooled region. Our results show that a KWW type ISF describes the water relaxation very effectively.

ACKNOWLEDGMENT

The authors would like to thank Collin Campbell for valuable discussions and assistance in scientific computing techniques.

[1] M.-C. Bellissent-Funel, K. F. Bradley, S.-H. Chen, J. Lal, and J. Teixeira, Physica A **201**, 277 (1993).
[2] M.-C. Bellissent-Funel, S.-H. Chen, and J.-M. Zanotti, Phys. Rev. E **51**, 4558 (1995).
[3] R. Holly, H. Peemoeller, C. Choi, and M. M. Pintar, J. Chem. Phys. **108**, 4183 (1998).
[4] S. Takahara *et al.*, J. Phys. Chem. B **103**, 5814 (1999).
[5] J.-M. Zanotti, M.-C. Bellissent-Funel, and S.-H. Chen, Phys. Rev. E **59**, 3084 (1999).
[6] M. A. Ricci and M. Rovere, J. Phys. IV **10**, Pr7-187 (2000).
[7] J. Swenson, R. Bergman, L. Borjesson, and W. S. Howells, J. Phys. IV **10**, Pr7-195 (2000).
[8] C. Czihak, M. Muller, H. Schober, and G. Vogl, J. Phys. IV **10**, Pr7-199 (2000).
[9] P. Gallo and M. Rovere, J. Phys. IV **10**, Pr7-203 (2000).
[10] H. N. Bordallo, K. W. Herwig, W. D. Dozier, and F. Drake, J. Phys. IV **10**, Pr7-207 (2000).
[11] V. Venuti, V. Crupi, S. Magazu, D. Majolino, P. Migliardo, and M.-C. Bellissent-Funel, J. Phys. IV **10**, Pr7-211 (2000).
[12] J. Teixeira, M.-C. Bellissent-Funel, S.-H. Chen, and A. J. Dianoux, Phys. Rev. A **31**, 1913 (1985).
[13] J. Swenson, R. Bergman, and S. Longeville, J. Chem. Phys. **115**, 11 299 (2001).
[14] P. Behrens and G. D. Stucky, Angew. Chem. Int. Ed. Engl. **32**, 696 (1993).
[15] J. Y. Ying, C. P. Mehnert, and M. S. Wong, Angew. Chem. Int. Ed. Engl. **38**, 56 (1999).
[16] K. Morishige and K. Kawano, J. Chem. Phys. **110**, 4867 (1999).
[17] K. Morishige and K. Nubuoka, J. Chem. Phys. **107**, 6965 (1997).
[18] D. Morineau, G. Dosseh, C. Alba-Simionesco, and P. Llewellyn, Philos. Mag. B **79**, 1847 (1999).
[19] C. Faivre, D. Bellet, and G. Dolino, Eur. Phys. J. B **7**, 19 (1999).
[20] F. Volino and A. J. Dianoux, Mol. Phys. **41**, 271 (1980).
[21] R. Schmidt, E. W. Hansen, M. Stocker, D. Akropiaye, and O. H. Ellestad, J. Am. Chem. Soc. **117**, 4049 (1995).
[22] P. M. Gehring and D. A. Neumann, Physica B **241-243**, 64 (1998).
[23] G. L. Squires, *Introduction to the Theory of Thermal Neutron Scattering* (Cambridge University Press, Cambridge, England, 1978).
[24] A. J. Dianoux, M. Pineri, and F. Volino, Mol. Phys. **46**, 129 (1982).
[25] W. Gotze, J. Phys.: Condens. Matter **11**, A1 (1999).
[26] S. H. Chen, C. Liao, F. Sciortino, P. Gallo, and P. Tartaglia, Phys. Rev. E **59**, 6708 (1999).
[27] R. Lamanna and S. Cannistraro, Phys. Rev. A **46**, 7367 (1992).
[28] O. A. Nabokov and Yu. A. Lubimov, Mol. Phys. **65**, 1473 (1988).
[29] Y. I. Naberukhin, J. Phys. A **19**, L681 (1986).
[30] H. E. Stanley, R. L. Blumberg, A. Geiger, P. Mausbach, and J. J. Teixeira, J. Phys. (Paris), Colloq. **45**, C7-13 (1984).
[31] H. E. Stanley and I. J. Teixeira, J. Chem. Phys. **73**, 3404 (1980).
[32] L. P. N. Rebelo, P. G. Debendetti, and S. J. Sastry, J. Chem. Phys. **109**, 626 (1998).
[33] M. Settles and W. Doster, Faraday Discuss. **103**, 269 (1996).
[34] R. Schmidt, E. W. Hansen, M. Stocker, D. Akropiaye, and O. H. Ellestad, J. Am. Chem. Soc. **117**, 4049 (1995).
[35] J. Colmenero, A. Arbe, A. Alegria, M. Monkenbusch, and D. Richter, J. Phys.: Condens. Matter **11**, A363 (1999).
[36] F. Sciortino, Chem. Phys. **258**, 307 (2000).
[37] F. Mansour and H. Peemoeller (unpublished).
[38] Manufacturers are identified in order to provide complete identification of experimental conditions, and such identification is not intended as a recommendation or endorsement by NIST.